August 1966

USCEE Report 128

# UNIVERSITY OF SOUTHERN CALIFORNIA

## SCHOOL OF ENGINEERING

# AN ASYNCHRONOUS PULSE-AMPLITUDE PULSE-WIDTH MODEL OF THE HUMAN OPERATOR



M. J. Merritt



ELECTRONIC SCIENCES LABORATORY

USCEE Report 128

Technical Report

# AN ASYNCHRONOUS PULSE-AMPLITUDE PULSE-WIDTH MODEL OF THE HUMAN OPERATOR

M. J. Merritt

ELECTRICAL ENGINEERING DEPARTMENT
UNIVERSITY OF SOUTHERN CALIFORNIA
LOS ANGELES, CALIFORNIA

March 1966

This research was sponsored by the National Aeronautics and Space Administration under Grant No. NGR-05-018-022

# INTRODUCTION

In order to develop a model for the behavior of a human operator performing a manual control task it is necessary to make some assumptions concerning the operator's inputs and outputs. If it is assumed that the operators utilizes the input continuously and produces continuous outputs then there are a wide variety of techniques which can be used to develop complete human operator models. The various techniques: spectral analysis ( 7, 11), linear combinations of orthogonal filters (13), and gradient search model identification (8) have been used extensively to study the behavior of human operators. Another assumption which has been studied is that the human operator samples the inputs periodically and produces continuous outputs. The physiology of the optical, neuro-muscular, and cerebral systems (9) supports this assumption. Sampling human operator models are difficult to identify due to the interactions between the sampling rate and time constants in the continuous portion of the model. For simple controlled elements (1, 2) and step inputs (5) complete human operator models have been identified.

Although the physiology supports the use of sampled data models for human operators, many studies have produced no evidence of periodic sampling behavior. In a recent study (7) the power spectrum of the model remnant was examined for periodicities corresponding to samp-

ling phenomena. No evidence of periodic sampling was found. A series of experiments were initiated in the System Simulation Laboratory of the University of Southern California to study the effects of small random perturbations about a nominal sampling interval on the power spectrum of the model remnant. With no perturbations, the power spectrum of the model remnant contained strong periodicities on either side of the sampling frequency. When the random perturbation was introduced the periodicities associated with sampling behavior were reduced in amplitude and broadened until the individual peaks were no longer detectable. The sampling behavior of human operators is certainly aperiodic and possibly controlled by a supervisory input monitor. This results in aperiodic input dependent sampling, which may also contain random variations in the sampling interval. If this is indeed the case, the model remnant would not contain strong periodicities.

When the dynamics of the controlled element are $1/s^2$ or higher, the performance of the human operator approaches that of a bang-bang system. In particular, the double integrator plant, $1/s^2$, usually elicits pulse responses from human operators (4, 6, 14).

Triangular pulse outputs are discrete events consisting of three tuple; time of pulse initiation, pulse amplitude, and pulse width. A mathmatical model to represent this output behavior could contain

sampled inputs with continuous supervisory control of the sampling. This supervisory sampling replaces the periodic sampling of Bekey (1, 2) with aperiodic input dependent sampling. The pulse nature of the output makes it possible to relate pulse events to decision surfaces in the error phase space (9, 15). The selection of suitable decision surfaces and the development of an input supervisory control element requires new computational tools.

The object of this paper is to describe the development of a human operator model which produces discrete pulse outputs in response to continuously presented gaussian random inputs. Computer procedures for the complete identification of all model parameters are described.

# I PRELIMINARY COMMENTS

A block diagram of the compensatory tracking situation used in this study is shown in Figure (1), and a portion of a typical tracking record is found in Figure (2). An examination of the human operator output (stick position) reveals a sequence of pulses which are roughly trangular in shape. For the purposes of this study, the actual human operator output is converted to the idealized human operator output, as seen in Figure (2). The selection of symmetric triangular pulses as ideal human operator pulses is arbitrary, and other pulse shapes can be used. Further, the decision to treat each pulse as a separate event, uncorrelated with previous pulses is in keeping with the basic nature of this study. The use of pre-programmed pulse sequences (3, 10, 12) presents an opportunity to extend the work presented below.

The transient human operator record is idealized into a sequence of three-tuples: time of the pulse initiation, pulse amplitude, and pulse width. If a causal relationship exists between the transient human operator inputs and the pulse outputs, then the input record can be reduced to samples of the input in the vicinity of the pulse initiation. The relationships between these samples and the pulse output is the desired result.

Since each event is treated independently, short term human

operator variations are easily computed. These variations are the differences between the model outputs and the actual human operator outputs. The distribution functions of these variations can be obtained and, if desired, can be re-inserted as model perturbations to produce a human operator model statistically indistinguishable from the actual human operator. The distribution functions and their associated parameters (mean and moments) can be used as measures of performance and state of training.

## II THE EXPERIMENT

The compensatory tracking situation shown in Figure (1A) was mechanized using a Beckman 2132 analog computer, an X-Y oscilloscope and side arm control stick. Operator distraction was minimized by placing the manual control station inside a sound proof enclosure with approximately 40 db of audio attenuation. The operator wore an aircraft type headset with lip microphone for communication purposes. The operator sat in a chair without armrests facing the display oscilloscope. The control stick was adjustable in position and contained an integral arm rest. The operator adjusted the control stick and arm rest into a comfortable position. The oscilloscope was placed at eye level.

The double integrator plant closely resembles an aircraft pitch axis. The input is elevator position and the output is altitude. In order

to preserve this resemblance, the error display selected is a rotating needle corresponding to a glide path indicator in an aircraft navigational /ILS display. Horizontal needle position represents zero error. The frequency response problems associated with actual instruments were avoided by simulating the glide slope needle with an oscilloscope containing a specially prepared edge lighted reticle.

The control stick and oscilloscope were connected to the analog computer which converted the stick output to a voltage, computed the plant response, and generated the necessary X and Y axis signals for the error display. By solving some of the equations explicitly it was possible to obtain the error and its exact derivative. The inputs to the system were obtained by filtering the output of a low frequency gaussian noise source. The filter transfer function was:

$$F(s) = \frac{K}{(10\,s + 1)\,(s+1)^3}$$

An FM magnetic tape recorder was used to record tracking data. Unfortunately, the tape recorder used in the experiments had only four data channels available. This necessitated some consolidation of the signals available in the analog computer. The signals recorded on magnetic tape were the error, its derivative, and the stick position.

A digital computer program was written for the IBM 1710 system to digitize these signals and store them on the IBM 1311 bulk storage

disk file. The analog to digital converters available in the USC System Simulation Laboratory commutate at 20 microseconds per channel. The execution time of the 1620 limits the rate at which the signals can be sampled to 100 samples per second. The sampling rate is controlled by the iterative clock of the analog computer. The clock is digitally set and counts pulses from a 100 KC crystal oscillator.

Practical considerations limited modeling to one subject. This is not restrictive in a study of this type as the techniques developed below would apply to any subject in any state of training. The difficulty is to select a model and establish that this model is a suitable one for the situation at hand. Once a model is selected and the feasibility of the computational schemes demonstrated, it becomes a simple matter to analyze new tracking data in both real time and off-line computational situations.

The subject received approximately 20 hours of training over a period of one month. The training sessions consisted of 10 minutes of tracking with 10 minute-rest periods. No data was taken during the early training sessions. The results of one of the last sessions were recorded on magnetic tape. From the 10 minute session approximately 3 minutes of data was subsequently digitized. The sampling interval utilized was 25 milliseconds or 40 samples per second.

## III PRELIMINARY ANALYSIS

A typical portion of the tracking record is seen in Figure (2).

The pulse nature of the stick output is clearly evident. As described above, it is possible to locate a discrete set of output events and attempt to establish a causal relationship between these events and some measures on the system.

An SPS program called MESS was written to call blocks of 10,000 digits of data into the common area of a Fortran program from the 1311 disk file. This program was necessary as there are no provisions in 1710 Fortran for addressing the disk file directly. The shear bulk of the data precluded any attempt to locate output pulses by hand. A Fortran program called STARTER was written to locate the beginning of pulses and their peak amplitudes.

The digitized data stored on the 1311 disk file was printed out and punched on IBM cards for permanent storage. Using the results of STARTER, the listing was examined and the following data was subsequently punched on IBM cards:

1. The time of the pulse initiation.
2. The time of the pulse termination.
3. The peak amplitude of the pulse.
4. The values of e and $\dot{e}$ at the following times :
   C. One sample after the initiation of the pulse.
   B. At the start of the pulse.
   A. The 5 samples prior to the start of the pulse.

STARTER located 160 pulse events in the digitized tracking record. For convenience, only the first 150 events were used below.

## IV HUMAN OPERATOR MODEL

In order to carry out detailed modeling efforts, a basic model structure must be hypothesized. The parameters of the model are then identified from experimental data and the model tested for validity. intuitive concepts of human operator behavior and an examination of the tracking record, Figure (2), led to the model shown in Figure (1B). From the early studies of the tracking record it appeared that the slope of the leading and trailing edges of the pulses were constant, corresponding to a constant velocity hand motion. If this were the case, pulse width would be proportional to pulse amplitude. This hypothesis is investigated below and is found to be only partially true. The pulse width is almost constant and only slightly dependent on pulse amplitude.

The amount of pulse amplitude modulation utilized by the human operator is evidenced in the distribution function of the pulse amplitudes, Figure (3). The amplitude modulation is clearly asymmetric.

## V PULSE AMPLITUDE-PULSE WIDTH RELATIONSHIPS

### I. Pulse Amplitude

The expected relationship between the inputs and the pulse amplitude is:

$$c_1\, e(t_i - \tau_1) + c_2\, \dot{e}\,(t_i - \tau_1) = p_i$$

where $c_1$ and $c_2$ are constants and $\tau_1$ is a time delay, all of which are to be determined, $t_i$ are the times at which the pulses started, e and $\dot{e}$ are the human operator input and its derivative.

The constants $c_1$ and $c_2$ are easily determined for fixed values of $\tau_1$. If there are N events (human operator pulses) then there are N equations in two unknowns (let $\tau_1^*$ represent the fixed values of $\tau_1$ to be used in the following equation):

$$p_1 = c_1\, e(t_1 - \tau_1^*) + c_2\, \dot{e}\ (t_1 - \tau_1^*)$$

$$p_2 = c_1\, e\,(t_2 - \tau_1^*) + c_2\, \dot{e}\ (t_2 - \tau_1^*)$$

$$\vdots$$

$$p_N = c_1\, e(t_N - \tau_1^*) + c_2\, \dot{e}\,(t_N - \tau_1^*)$$

or, in vector form

$$p = Ac$$

where A is an N × 2 matrix of the values of e and $\dot{e}$. A least squares error criterion is:

$$\phi = (p - Ac)^T (p - Ac)$$

which is a positive definite quadratic function of the parameter vector, c. In expanded form.

$$\phi = p'p - 2c'A'p + c'A'Ac.$$

The gradient of the criterion function is:

$$\frac{\partial \phi}{\partial c} = 2A'p + 2A'Ac$$

A stationary point of the criterion function is found by setting:

$$\frac{2\emptyset}{2c} \equiv 0$$

yielding

$$A'Ac = A'p$$

finally

$$c = [\, A'A \,]^{-1} A'p$$

The parameter vector, c, which results from this computation represents those values of $c_1$ and $c_2$ which produce the best least squares fit between $c_1 e(t_i - \tau_1^*) + c_2 \dot{e}(t_i - \tau_1^*)$ and the pulse amplitude for a given value of $\tau_1$ say $\tau_1^*$.

The criterion function, $\emptyset$, is a measure of the correlation between the model relationship and the experimental data. In order to gain more insight into the problem, the values of $c_1 e(t_i - \tau_1^*) + c_2 \dot{e}(t_i - \tau_1^*)$ were plotted against the actual pulse amplitude for each of the 150 pulse events. If the human operator were invariant with time and the model an exact representation, this plot would produce a straight line with a slope of one, corresponding to a criterion function of zero. There are two ways in which the optimal value for $\tau_1$ can be selected from the set of values $\tau_1^*$ used in the linear regression routine above. The first would be to examine the point plots just described for various values of $\tau_1^*$ selecting that plot which produced the best visual approximation to a perfect straight line. The second method is to select that value of $\tau_1^*$ which produces the minimum criterion function, $\emptyset$. Both methods

will be used below in analyzing and interpreting the results from the least squares linear regression analysis.

Regardless of the method of selection, once an optimal value for $\tau_1$ has been selected from the set of values $\tau_1^*$ the values of $c_1$ and $c_2$ corresponding to that value of $\tau_1^*$ can be obtained. The values of K and T used in the model of Figure 1B can be computed since:

$$K = c_1$$

$$T = c_2/c_1$$

$$T_1 = (T_1^*) \text{ Optimal}$$

## COMPUTER RESULTS

The limited memory capacity of the 1710 computer made it difficult to study all of the 150 pulse events at one time, thus only the first 100 events were used. Starting 125 milliseconds before the initiation of the pulse and progressing in 25 millisecond steps to 25 milliseconds past the initiation of the pulse, the values of e and $\dot{e}$ were punched on IBM cards. In addition the amplitude of the pulse was punched. These IBM cards were used as inputs for the last squares linear regression analysis described above. The computational results are tabluated in Table I. The seven samples correspond to a range of time delays from 125 to -25 milliseconds relative to the start of the pulse.

From Table I it is seen that the optimum parameter values are

$c_1 = -0.163$, $c_2 = -0.290$ and $\tau_1 = 0.100$ seconds. A plot of $c_1 e^{(t_i - 0.100)} + c_2 e^{(t_i - 0.100)}$ versus pulse amplitude for $1 \leq i \leq 100$ is found in Figure 4. A visual inspection of this figure reveals a number of interesting anomalies. The distribution of points is considerably different for

TABLE I

| $\tau_1^*$ | $c_1$ | $c_2$ | $\phi \times 10^{-6}$ |
|---|---|---|---|
| .125 | -.162 | -.302 | 1.391 |
| .100 | -.163 | -.290 | 1.358 |
| .075 | -.164 | -.279 | 1.359 |
| .050 | -.165 | -.268 | 1.387 |
| .025 | -.165 | -.257 | 1.446 |
| 0 | -.167 | -.246 | 1.529 |
| -.025 | -.172 | -.235 | 1.619 |

the two sets of pulse events. The negative pulses in quadrant 3 show a significant linear relationship with an offset towards the negative x-axis. The positive pulses, quadrant 1, on the other hand, show no clear linear trend although containing an offset towards the positive x-axis. In analyzing both the positive and negative pulses simultaneously the linear regression routine attempts to cancel the effect of the offsets by placing the center of gravity of the points at the origin. This may be overcome by regressing on the two sets of pulse events separtely. Separating the pulse events into two groups yields 76 positive pulses and 74 negative pulses. The linear regression routine will accept up to 100

events, thus allowing all 150 events digitized to be included in the analysis. Table 2 represents the results of using the same equation:

$$c_1 e (t_i - \tau_1^*) + c_2 \dot{e} (t_i - \tau_1^*) = p_i$$

on each group of pulses separately.

TABLE 2

| $\tau_1^*$ | $c_1$ | | $c_2$ | | $\phi \times 10^{-6}$ | |
|---|---|---|---|---|---|---|
| Polarity of Pulse | + | - | + | - | + | - |
| .125 | -.183 | -.167 | -.323 | -.287 | 1.231 | .602 |
| .100 | -.183 | -.166 | -.308 | -.277 | 1.235 | .578 |
| .075 | -.185 | -.166 | -.294 | -.267 | 1.228 | .587 |
| .050 | -.185 | -.166 | -.281 | -.257 | 1.234 | .621 |
| .025 | -.183 | -.167 | -.268 | -.245 | 1.270 | .665 |
| 0 | -.183 | -.170 | -.257 | -.235 | 1.330 | .703 |
| -.025 | -.187 | ——— | -.244 | ——— | 1.371 | ——— |

The optimum values for the positive and negative pulses, respectively are: $c_1 = -0.185, -0.166$, $c_2 = -0.294, -0.277$, and $\tau_1 = 0.75, 0.100$. In Figure 7 is found a graph of the criterion function $\phi$ versus $\tau_1^*$. From this graph it can be seen that the changes in criterion function with $\tau_1^*$ although not large are significant. The minimums in both cases are well defined. A visual measure of the correlation between the experimental data points and the model equation can be obtained by plotting $c_1 e + c_2 \dot{e}$ versus pulse amplitude for the optimal parameter values indicated above;

such a graph is found in Figure 5. Although the groupings found in Figure 5 are somewhat better than those found in Figure 4, the overall structure is not greatly changed. The X axis offsets are still apparent and somewhat better defined that they were in Figure 4.

In an attempt to obtain a model relationship which would produce better values of the criterion function by removing the offsets observed in Figures 4 and 5 the following model equation was selected:

$$c_1 e^{(t_i - \tau_1^*)} + c_2 e^{(t_i - \tau_1^*)} + c_3 = p_i$$

The least squares linear regression routine was rewritten to obtain the optimum parameter values for this equation. The results of these computations are tabulated in Table 3 and plotted in Figures 6 and 7.

TABLE 3

| $\tau_1^*$ | $c_1$ | | $c_2$ | | $c_3$ | | $\emptyset \times 10^{-6}$ | |
|---|---|---|---|---|---|---|---|---|
| Polarity | + | - | + | - | + | - | + | - |
| 0.125 | -0.060 | -0.065 | -0.139 | -0.145 | 2.16 | -2.02 | 0.507 | 0.220 |
| 0.100 | -0.061 | -0.066 | -0.134 | -0.143 | 2.16 | -1.99 | 0.496 | 0.217 |
| 0.075 | -0.062 | -0.065 | -0.130 | -0.137 | 2.16 | -2.00 | 0.495 | 0.222 |
| 0.050 | -0.062 | -0.064 | -0.125 | -0.131 | 2.16 | -2.04 | 0.492 | 0.228 |
| 0.025 | -0.059 | -0.061 | -0.118 | -0.123 | 2.19 | -2.10 | 0.498 | 0.242 |
| 0 | -0.057 | -0.060 | -0.112 | -0.116 | 2.22 | -2.14 | 0.504 | 0.253 |
| -0.025 | -0.057 | -0.060 | -0.106 | -0.108 | 2.25 | -2.20 | 0.509 | 0.263 |

The criterion function, $\emptyset$, versus $\tau_1^*$ is found in Figure 7. From this figure it can be seen that the minimums are again well defined. The scatter plot of $c_1 e + c_2 \dot{e} + c_3$ versus pulse amplitude is found in Figure 6. The groupings are quite close to the ideal unity slope line. The symmetry in the optimum parameter values for positive and negative pulses is contrasted with the considerable asymmetry observed above. The optimum values for positive and negative pulses, respectively are $c_1 = -0.062, -0.066$; $c_2 = -0.125, -0.143$; $c_3 = 2.16, -1.99$; and $\tau_1 = 0.050, 0.100$. The criterion function $\emptyset$ is a factor of three better than in all previous results. As is evidenced in all of the above results, the positive pulses produced poorer correlation than the negative pulses. This may be a result of one or more of the following factors: arm motion assymetry associated with the side arm control stick, incomplete training, or the tendency of the operator to prefer certain portions of the error phase plane (also a well-known result of incomplete training.)

An analysis of the differences between human operator amplitude and the corresponding model pulse amplitudes serves two purposes. The accuracy of the model may be measured and the distribution function of the human operator variations may be determined. These distribution functions are seen in Figure 8. The mean and standard deviation of these functions are:

TABLE 4

| | Pulse Polarity | |
|---|---|---|
| | + | - |
| Mean (volts) | 0 | 0 |
| Standard Deviation (volts) | 0.80 | 0.58 |

The amplitudes of human operator pulses range from 0.5 to 6.0 volts, with a distribution function as shown in Figure 3. One standard deviation represents about 40% error. Alternatively, noise of the same mean and standard deviation or the same distribution function could be added to the pulse amplitude model output.

II. Pulse Width:

Preliminary analysis of the tracking records led to the hypothesis that the pulse width was proportional to the pulse amplitude. The results below indicate that this is not necessarily the best model structure. A future study might consider the pulse width as another degree of freedom which is determined independently of pulse amplitude. A plot of pulse width versus pulse amplitude for each of the 150 events is found in Figure 9. The pulse width appears to be independent of pulse amplitude. Least squares linear regression was used to determine the optimal parameter values in the following equation:

$$c_1 p_i + c_2 = pw_i$$

The positive and negative pulses were treated separately. The optimal parameter values are $c_1 = -0.0205$, $-0.492$ and $c_2 = 0.7110$, $0.3157$. A visual estimate of the accuracy of this relationship is obtained by plotting $c_1 p_i + c_2$ versus $pw_i$, Figure 10A and B. If the pulse width were independent of pulse amplitude, the result would be a horizontal line. The spread is caused by the random human operator variations. The slope is caused by the slight dependence on pulse

amplitude. The differences between the human operator and the model outputs were computed. The mean and standard deviation of these differences are:

TABLE 5

| | Pulse Polarity | |
|---|---|---|
| | + | - |
| Mean (sec.) | 0 | 0 |
| Standard Deviation (sec.) | 0.05 | 0.04 |

The values of $pw_i$ range from 0.3 to 0.9 seconds. One standard deviation represents a maximum error of 16%. The distribution functions of these differences are found in Figure 11. As with the pulse amplitude model, the output of the pulse width model could be perturbed by random noise possessing the distribution function of Figure 11.

## PULSE INITIATION

The results of the pulse amplitude model clearly demonstrate the ability of the human operator to estimate the derivative of displayed signals. The pulse initiation decision model is based on this ability and the intuitive feeling that the human operator utilized a control policy which results in a relatively simple decision surface in the error phase space. A number of error phase plane trajectories were sketched, Figure 12. The trajectories start (circles) at the termination of a pulse event and and end (crosses) at the initiation of the next pulse. The human operator

appears to utilize the favorable error rate in the second and fourth quadrants by allowing the system to coast until the magnitude of the error is sufficiently small. If at that time, the error rate is still large, a new pulse event occurs. The human operator exhibits an error-error rate dead zone, inside of which no pulse events are generated. This is consistent with other human operator tracking experiments [1,15]. The decision to initiate a pulse and the actual pulse event will be separated by the reaction time of the human operator. Starting at the end of a human operator pulse, the e and $\dot{e}$ time histories are continuously monitored by a decision element. The time at which the decision element produces an output is computed and the time at which the human operator produced a pulse is available. The average difference between the two times should be the human operator reaction time. The spread of the time differences is a measure of the accuracy of the decision element. Idealy, all of the time differences would be the same. In practice the human operator variations and incorrect decision elements combine to spread the differences.

The treatment of each pulse as an individual event places restrictions on the decision element. A number of investigators [1, 2, 7, 9, 10, 15] have determined human operator times to be between 150 and 300 milliseconds. In Figure 13 is found the distribution function of the times between pulses. There are a large number of pulses spaced less than 200 milliseconds apart. These pulses probably correspond to pre-programmed pulse sequences [3, 12]. The human operator generates single pulses (rate corrections) and

pulse sequences (position corrections). A continuation of this study would include a pulse program decision element as described by Bekey and Angel [3]. With this limitation in mind, the identification of the decision element was undertaken.

Inspection of the error phase plane trajectories, Figure 13, led to the following pulse initiation model:

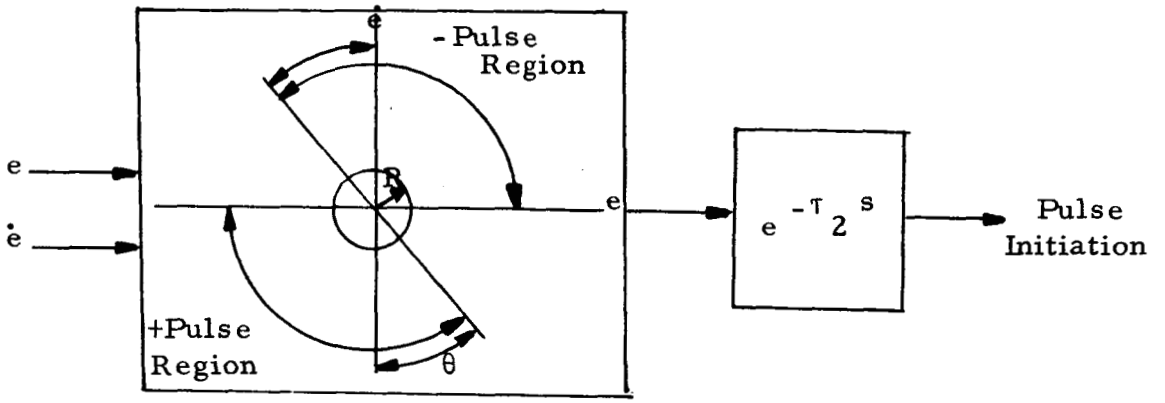


The following criterion function was selected in accordance with the verbal description above:

$$\phi(R, \theta) = \sum_{i=1}^{150} \left[ \tau_2 - (t_i - t_{im}) \right]^2$$

$$\tau_2 = \frac{1}{150} \sum_{i=1}^{150} (t_i - t_{im})$$

$\tau_2$ is the mean prediction time, $t_i$ and $t_{im}$ are the times at which the human operatior and the human operator model initiated pulses, respectively for $1 \leq i \leq 150$. The criterion function is the variance of the differences between mean prediction time and the actual prediction

time. The resultant value of $\tau_2$ is the human operator reaction time.

A systematic study of the R, $\theta$ parameter plane was conducted. The computational results of this optimum search are found in Figure 14. The optimum parameter values are R = 4.0 volts, $\theta = 35^\circ$ and $\tau_2$ = 0.200 sec. The distribution of differences between model pulse initiation and human operator pulse initiation times is found in Figure 15. The peak at 100 milliseconds late is probably due to preprogrammed pulse sequences. The use of more complex decision elements is clearly indicated. However, these results demonstrate the applicability of discrete decision elements to the development of input dependent sampling human operator models.

## THE COMPLETE HUMAN OPERATOR MODEL

The complete human operator model is shown in Figure 16 A. The parameters of this model have been identified as described above. The completely identified human operator model for one well trained subject is found in Figure 16 B

## CONCLUSIONS

The parameters of the human operator model shown in Figure 16 A were identified from experimental data taken from one subject in an advanced state of training, as evidenced by the absence of incorrect pulse responses in the tracking record studied. No records were made of the error or measures of the error as a function of training. The

state of training can only be estimated from the examination of the records and the subjects comments. The computational results brought to light a number of interesting results:

(1) The human operator reaction time of 200 milliseconds is in excellent agreement with other studies, [1, 2, 7, 9, 10, 15, ].

(2) The numerical values for the time delays in Figure 16B lead to the following logical sequence: (1) A decision is made to generate a pulse, (2) pause for 100 -150 milliseconds, (3) sample e (t) and $\dot{e}$ (t), (4) during the next 50-100 milliseconds compute the amplitude and width of the pulse, (5) generate the pulse.

(3) The pulse amplitude and pulse width models for negative pulses produce better correlations with the experimental data than for positive pulses. This is clearly apparent in the scatter plots, Figures 4, 5, 6, and 10, and in the values of the criterion function $\emptyset$, Figure 7. This may be the result of incomplete training, the design of the side arm controller used, the position of the subjects arm relative to the controller or a characteristic of the particular human operator in this experiment.

(4) The pulse amplitude models for positive and negative pulses are quite similar, despite considerable assymmetry in pulse amplitude distributions, Figure 3.

(5) The results presented in Figure 13 strongly indicate that human operators utilize pre-programmed pulse sequences.

(6) If the differences between model results and experimental tracking data are viewed as the result of short term human operator variations, then the statistics of the human operator variations are easily determined, [tables 4 and 5, and Figures 8 and 11].

From the present study it is not feasible to determine whether the model errors observed are random or functionally dependent on the human operator inputs and input-output history. Further studies should include pre-programmed pulse elements and more complex error phase plane decision surfaces. It would also be interesting to study the parameter changes and their associated distribution functions during training and as performance measures.

## REFERENCES


1. Bekey, G. A. "Sampled Data Models of the Human Operator in a Control System", Ph. D. dissertation, University of California at Los Angeles, 1962.

2. Bekey, G. A., "The Human Operator as a Sampled Data System", IRE Transactions, Vol. HFE-3, No. 2, Sept. 1962

3. Bekey, G. A., and Angel, E. S., "Asynchronous Finite State Models of Manual Control Systems", University of Southern California, Electronic Sciences Laboratory Report USCEE-160, 1966.

4. Elkind, J. I., Kelly, J. A., and Payne R. A., "Adaptive Characteristics of the Human Controller in Systems Having Complex Dynamics", Proceedings of the Fifth National Symposium on Human Factors in Electronics, 1964

5. Fu, K. S., and Knoop, D. E., "An Adaptive Model of the Human Operator in a Control System", Purdue University Report TREE 64-15, 1964.

6. Kelley, Charles R., "Design Applications of Adaptive (Self Adjusting) Simulators", Proceedings of NASA-MIT Working Conference on Manual Control, Feb. 28-March 2, 1966.

7. McRuer, D. and Graham, D., "Human Pilot Dynamics in Compensatory Systems", Technical Report No. AFFDL-TR-65-15.

8. Meissinger, H. F. and Bekey, G. A., "An Analysis of Continuous Parameter Identification Methods", Simulation, Feb. 1966.

9. Pew, Richard W., "Temporal Organization in Skilled Performance", University of Michigan Technical Report 02814-11-T, 1963

10. Pew, Richard W., "Performance of Human Operators in a Three-State Relay Control System with Velocity-Augmented Displays", IEEE Transactions on Human Factors in Electronics, Vol. 7 No. 2 June 1966.

11. Todosiev, E. P., Rose, R. E., Bekey, G. A., and Williams, H. L., "Human Tracking Performance in Uncoupled and Coupled Two Axis Systems", TRW Systems Report 4380-6003-R0000, 1965.

12. Tomovic, R. and McGhee, R. B., "A Finite State Approach to the Synthesis of Bioengineering Systems", IEEE Transactions on Human Factors in Engineering. Vol. 7 No. 2, June 1966.

13. Wierwille, W. W., "A theory for Optimal Deterministic Characterization of Time Varying Human Operator Dynamics", Cybernetics, Human Factors, IEEE Convention Record, Part 6, 1965.

14. Young, L. R. and Meiry, J. L., "Manual Control of an Unstable System with Visual and Motion Cues", IEEE Convention Record, Part 6, 1965.

15. Young, L. R. and Stark, L. "Biological Control Systems- A Critical Review and Evaluation", NASA Contractor Report CR-190, 1965.

# ILLUSTRATIONS

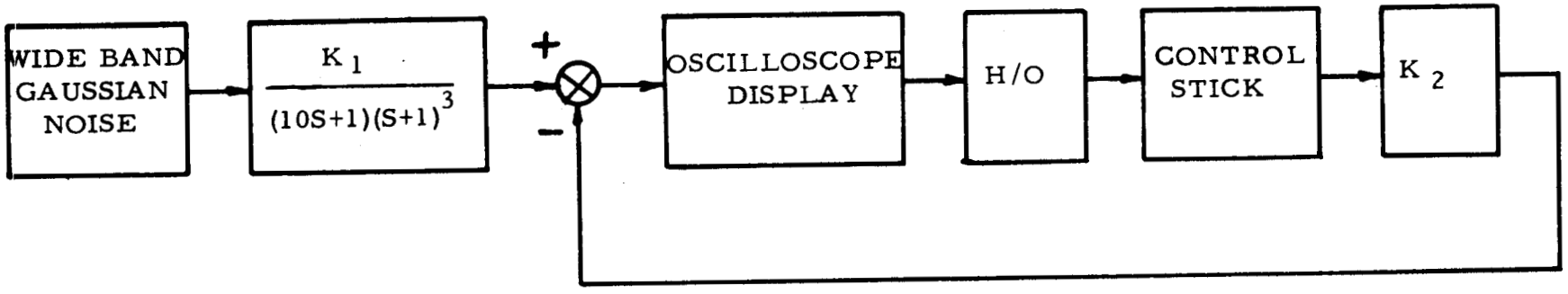


FIGURE 1A - COMPENSATORY TRACKING SYSTEM

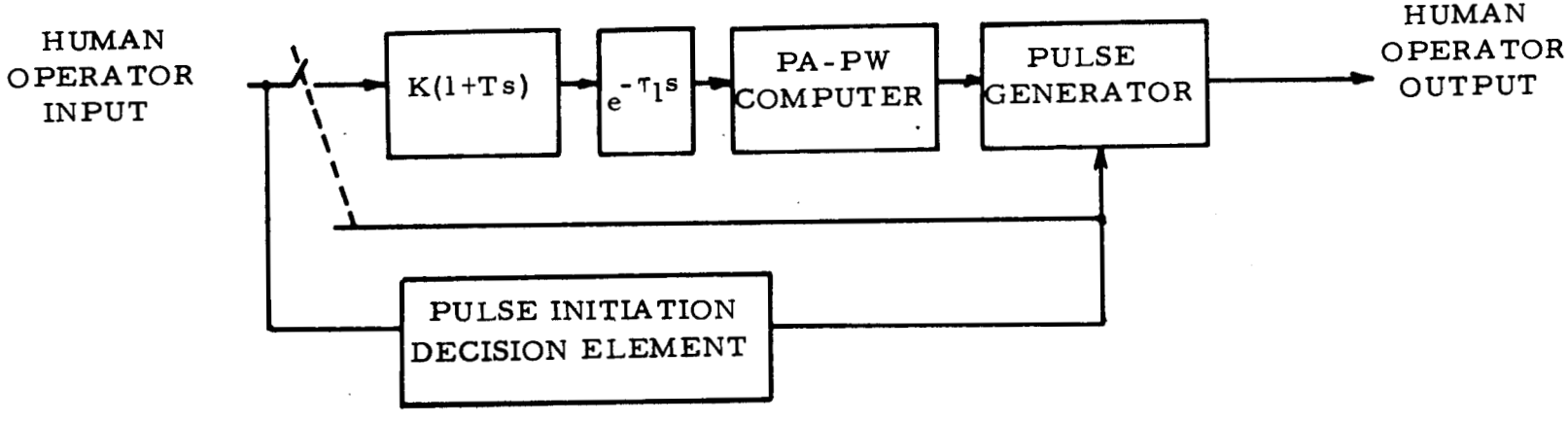


FIGURE 1B - GENERAL FORM OF PROPOSED HUMAN OPERATOR MODEL

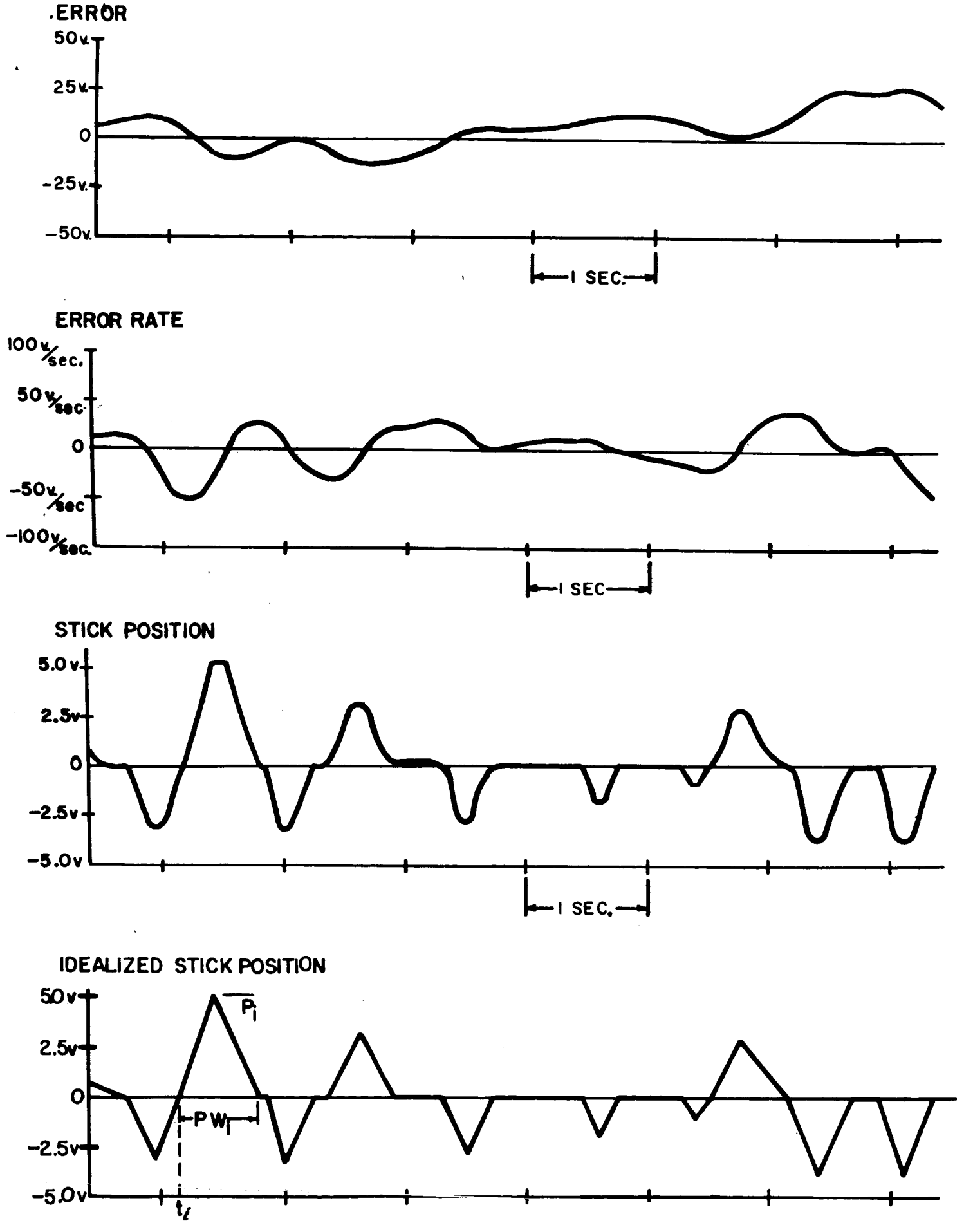


FIGURE 2 TYPICAL TRACKING RECORD

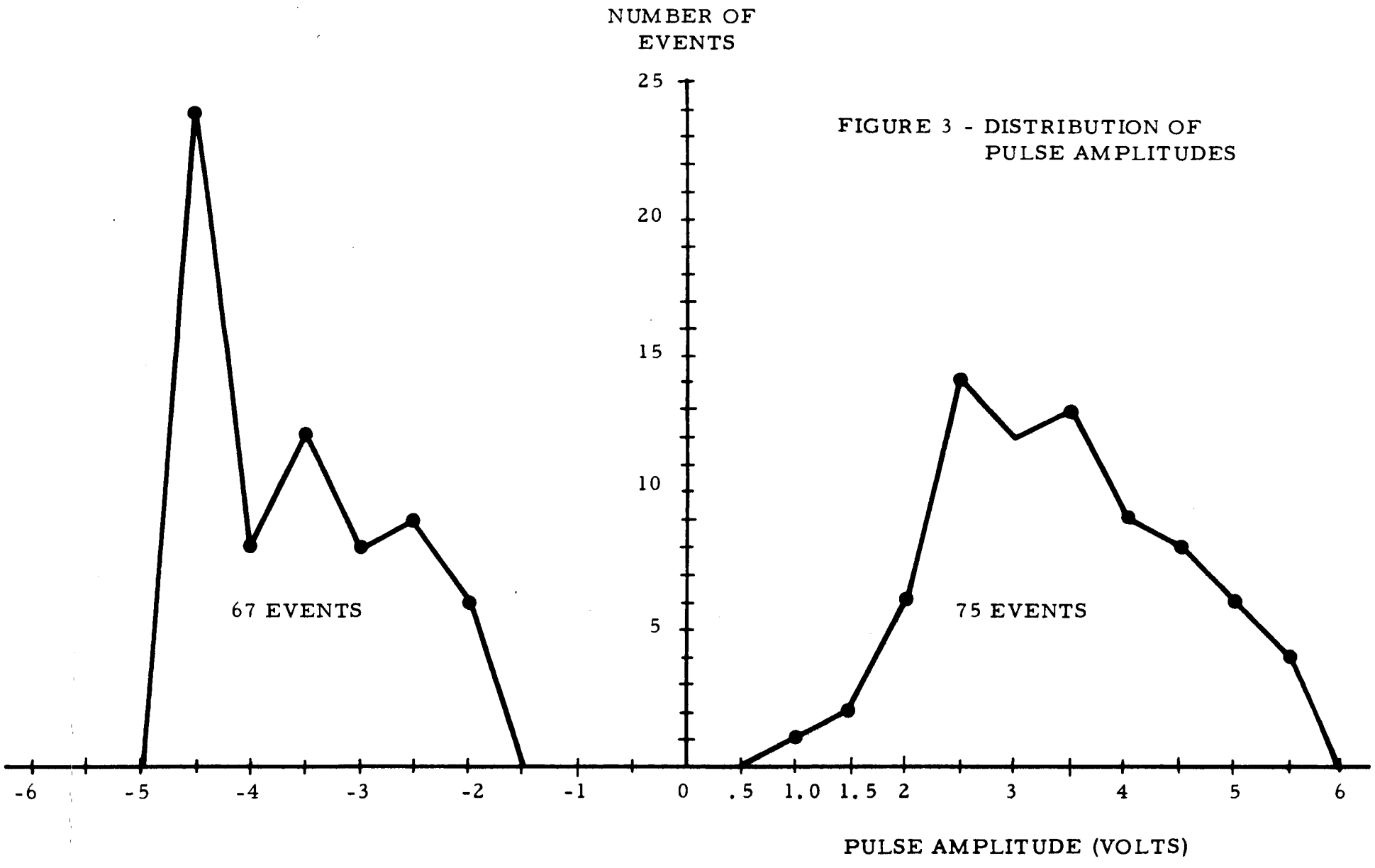


FIGURE 3 - DISTRIBUTION OF PULSE AMPLITUDES

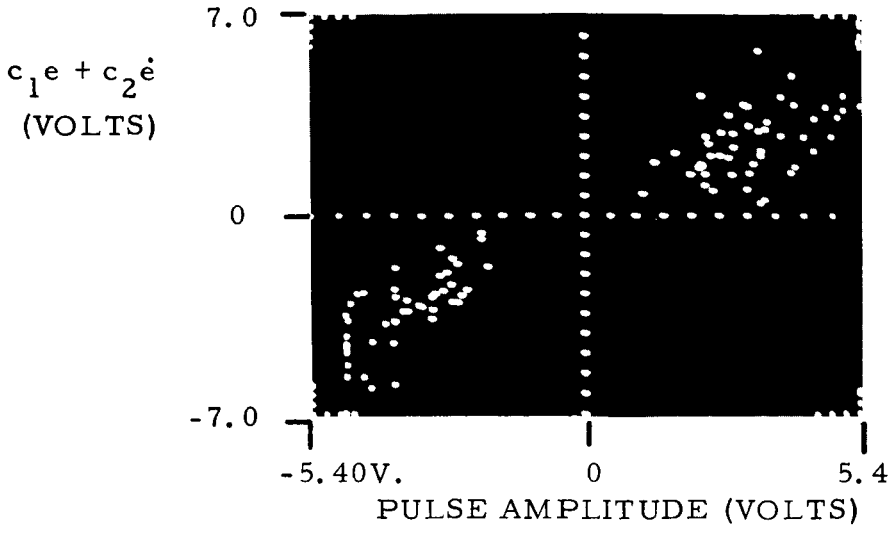


FIGURE 4 - $c_1e + c_2\dot{e}$ Vs PULSE AMPLITUDE FOR OPTIMAL PARAMETER VALUES

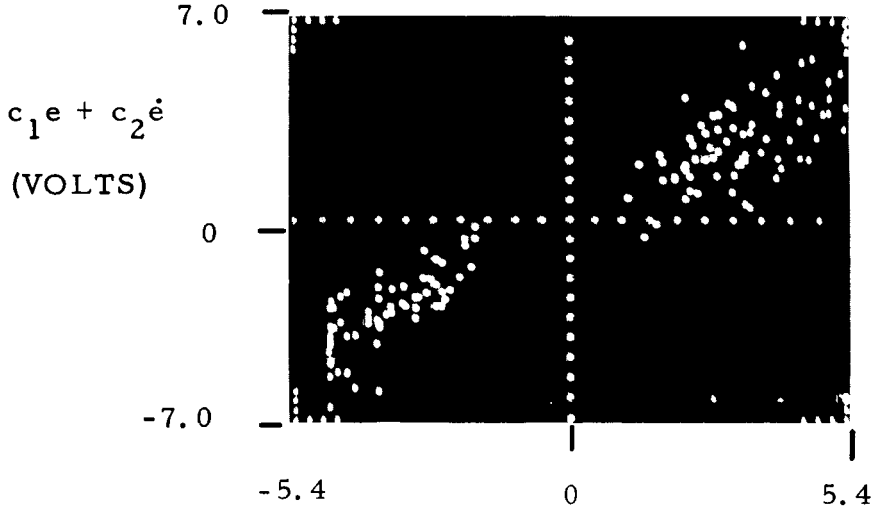


FIGURE 5 - $c_1e + c_2\dot{e}$ Vs PULSE AMPLITUDE, POSITIVE AND NEGATIVE PULSES OPTIMIZED SEPARATELY

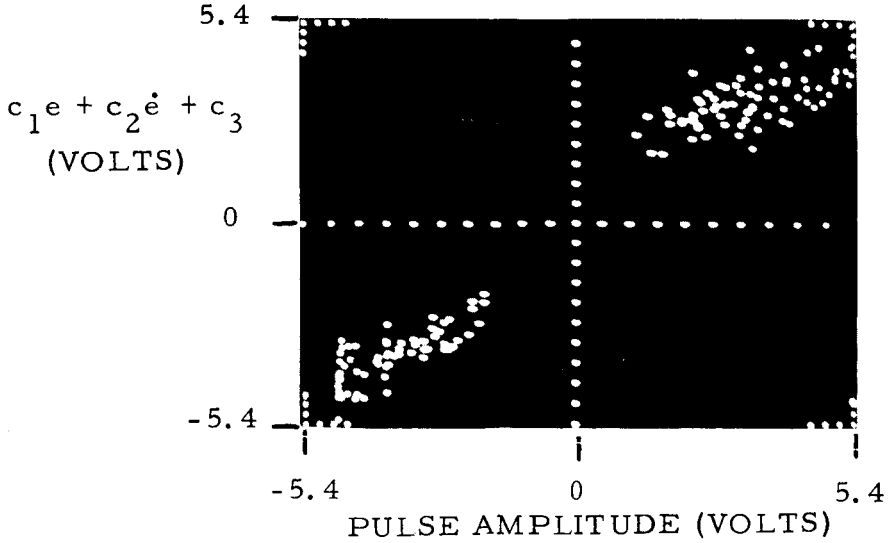


FIGURE 6 - $c_1e + c_2\dot{e} + c_3$ Vs PULSE AMPLITUDE, POSITIVE AND NEGATIVE PULSES OPTIMIZED SEPARATELY

FIGURE 7 - PULSE AMPLITUDE CRITERION FUNCTION Vs TIME DELAY

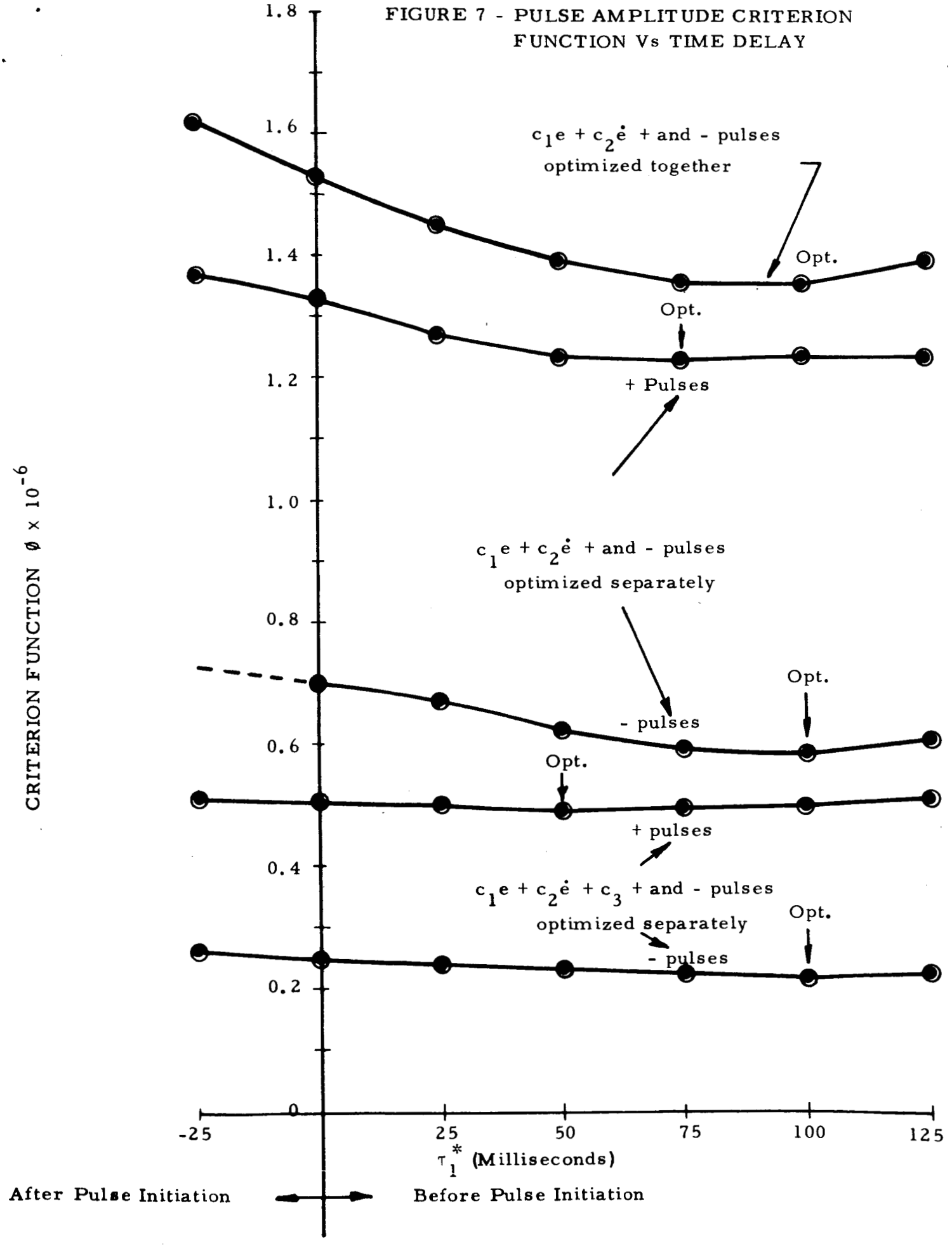

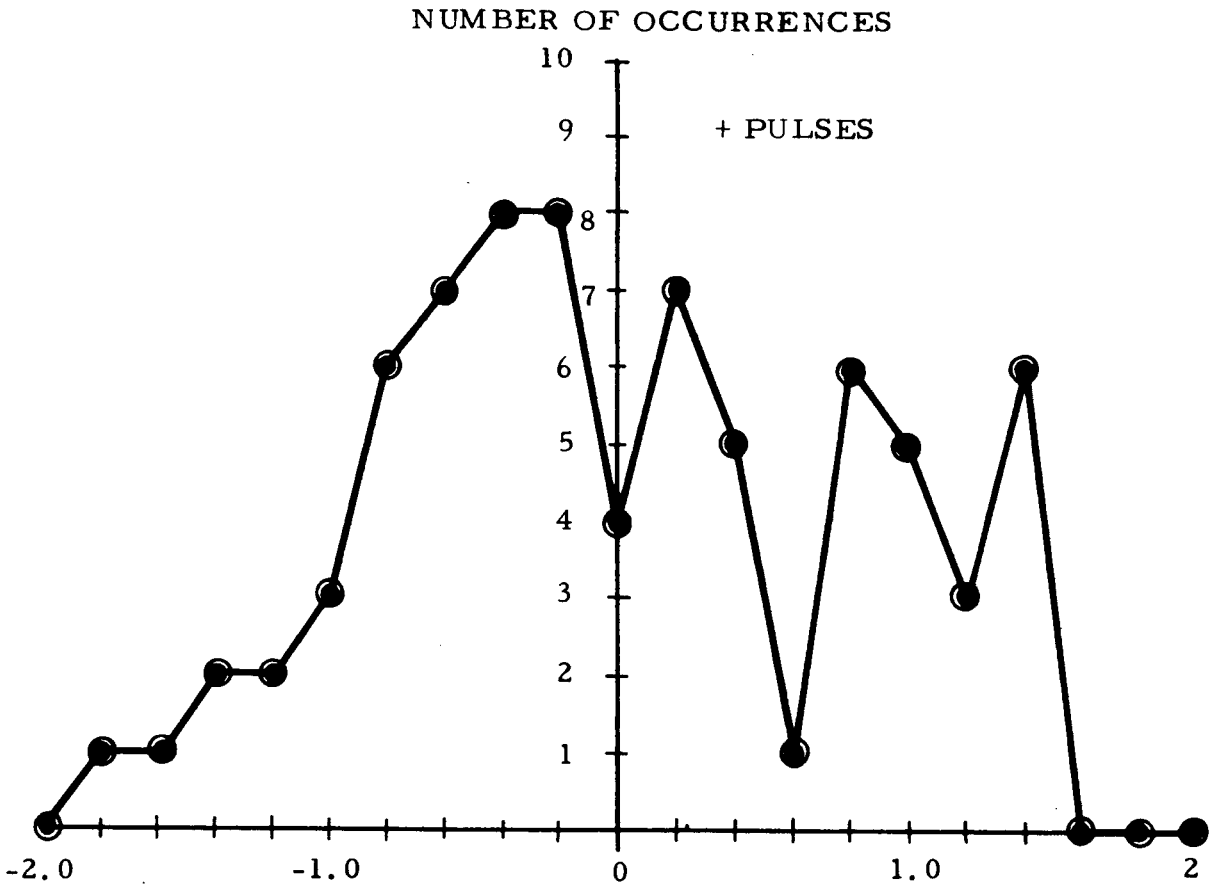


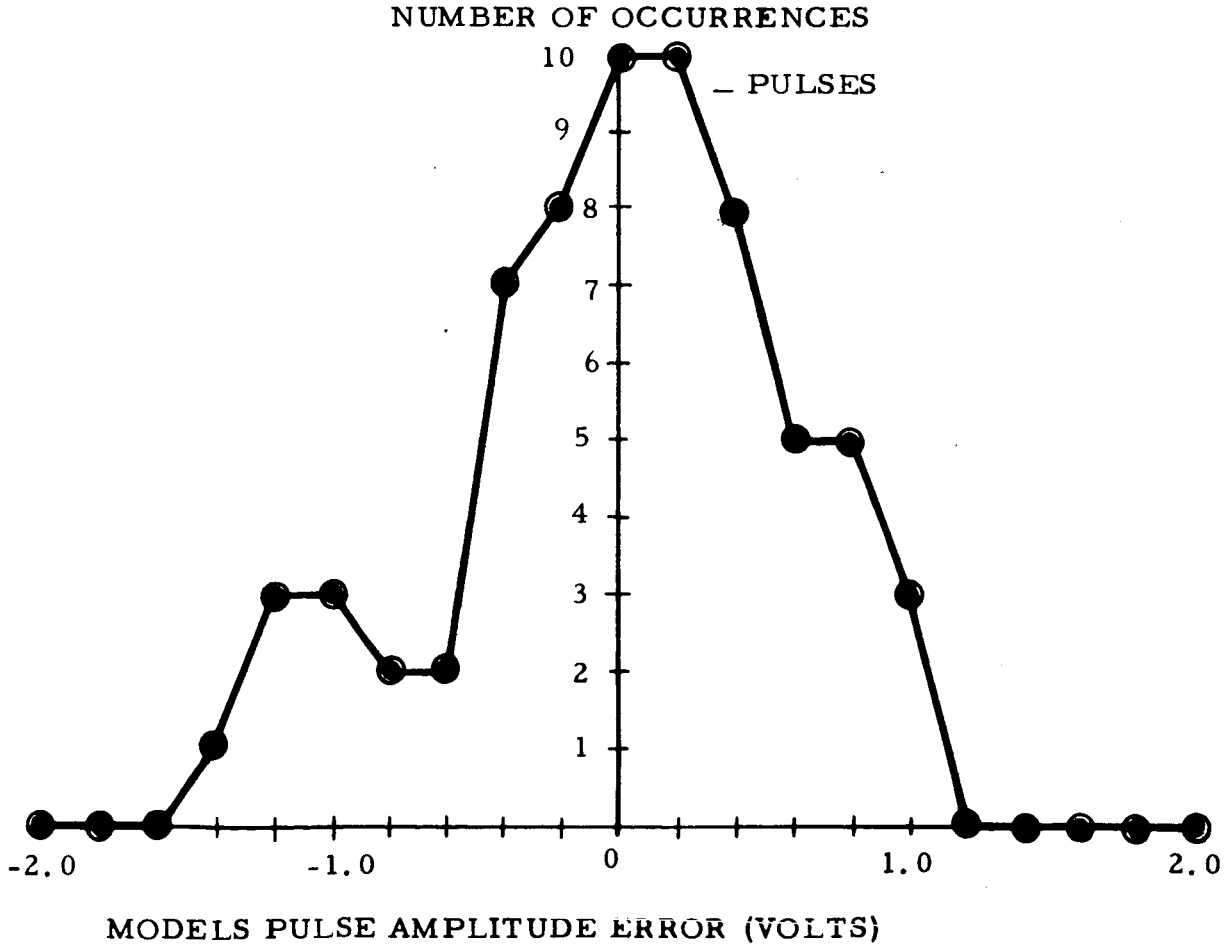


FIGURE 8 - DISTRIBUTION FUNCTIONS OF MODEL PULSE AMPLITUDE ERRORS

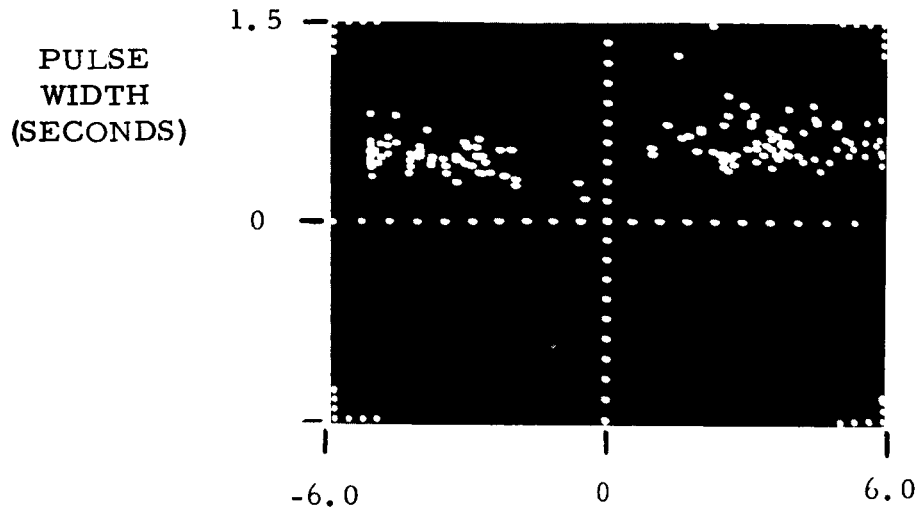


FIGURE 9 - PULSE WIDTH Vs PULSE AMPLITUDE

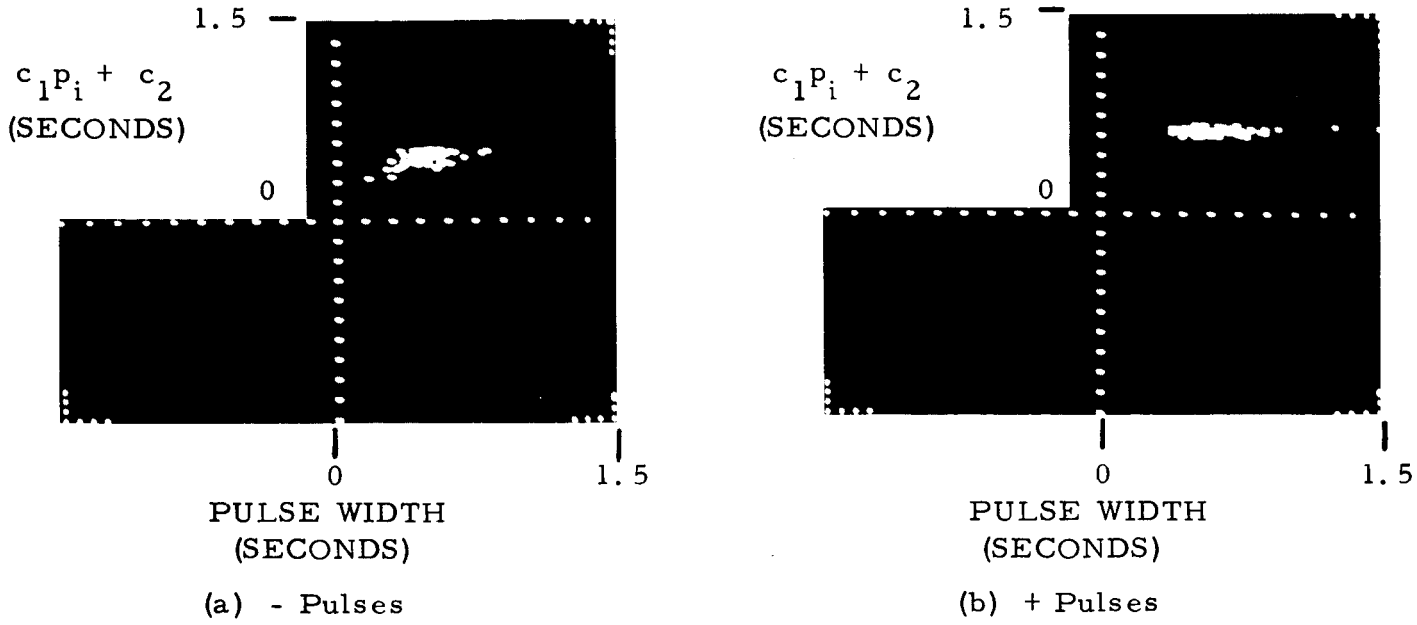


FIGURE 10 - MODEL PULSE WIDTH Vs ACTUAL PULSE WIDTH

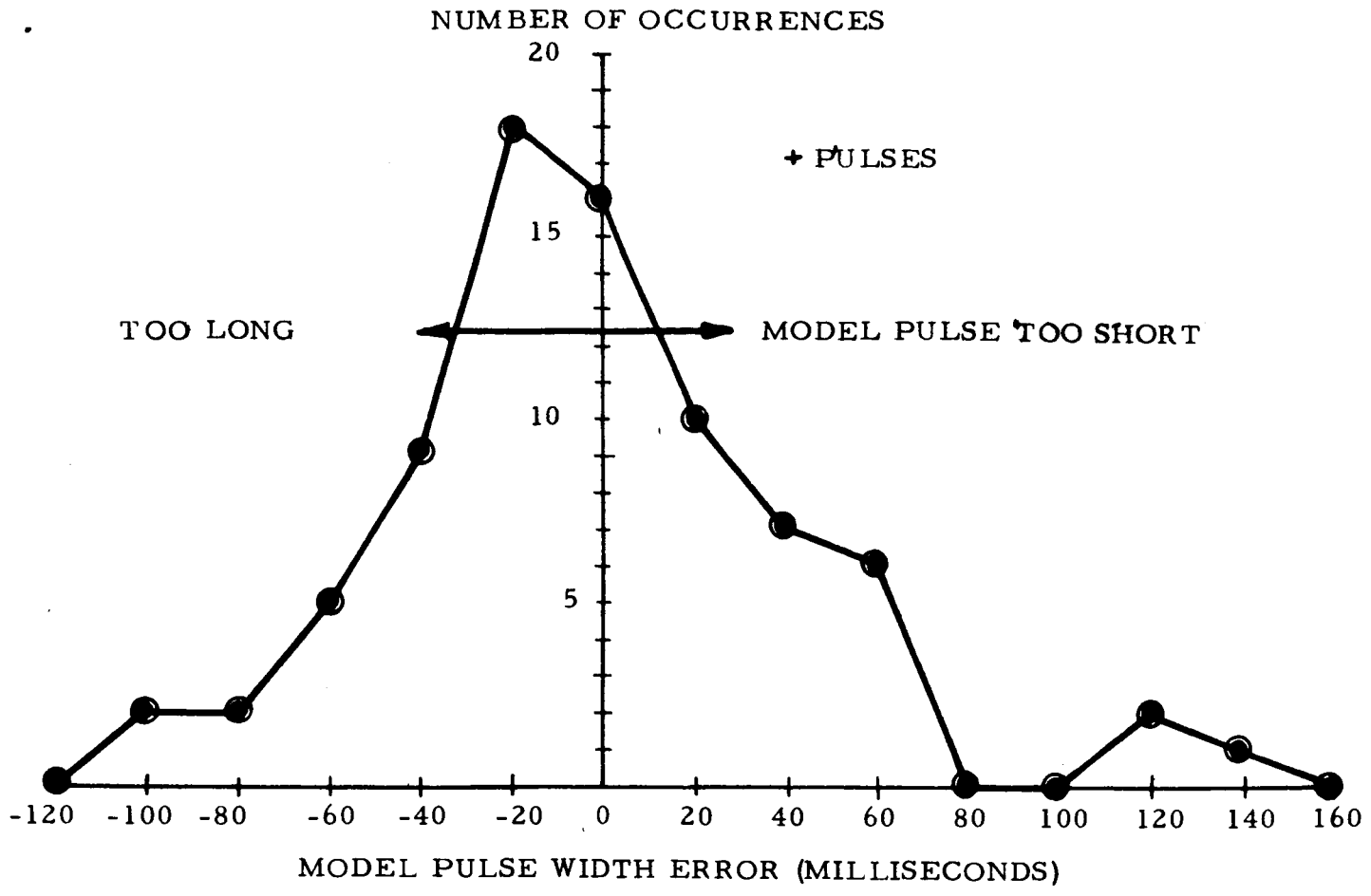


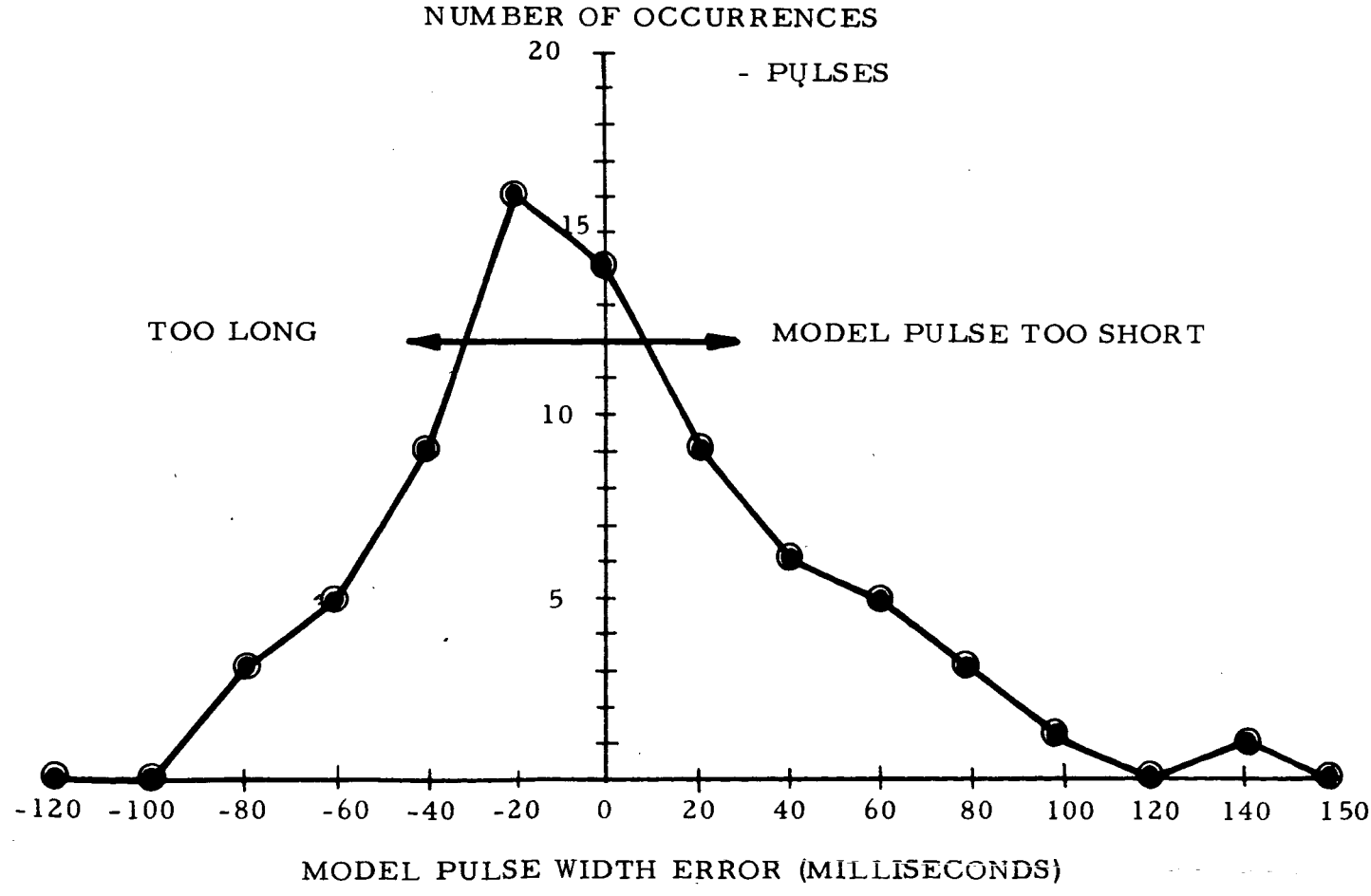


FIGURE 11 - DISTRIBUTION FUNCTIONS OF MODEL PULSE WIDTH ERRORS

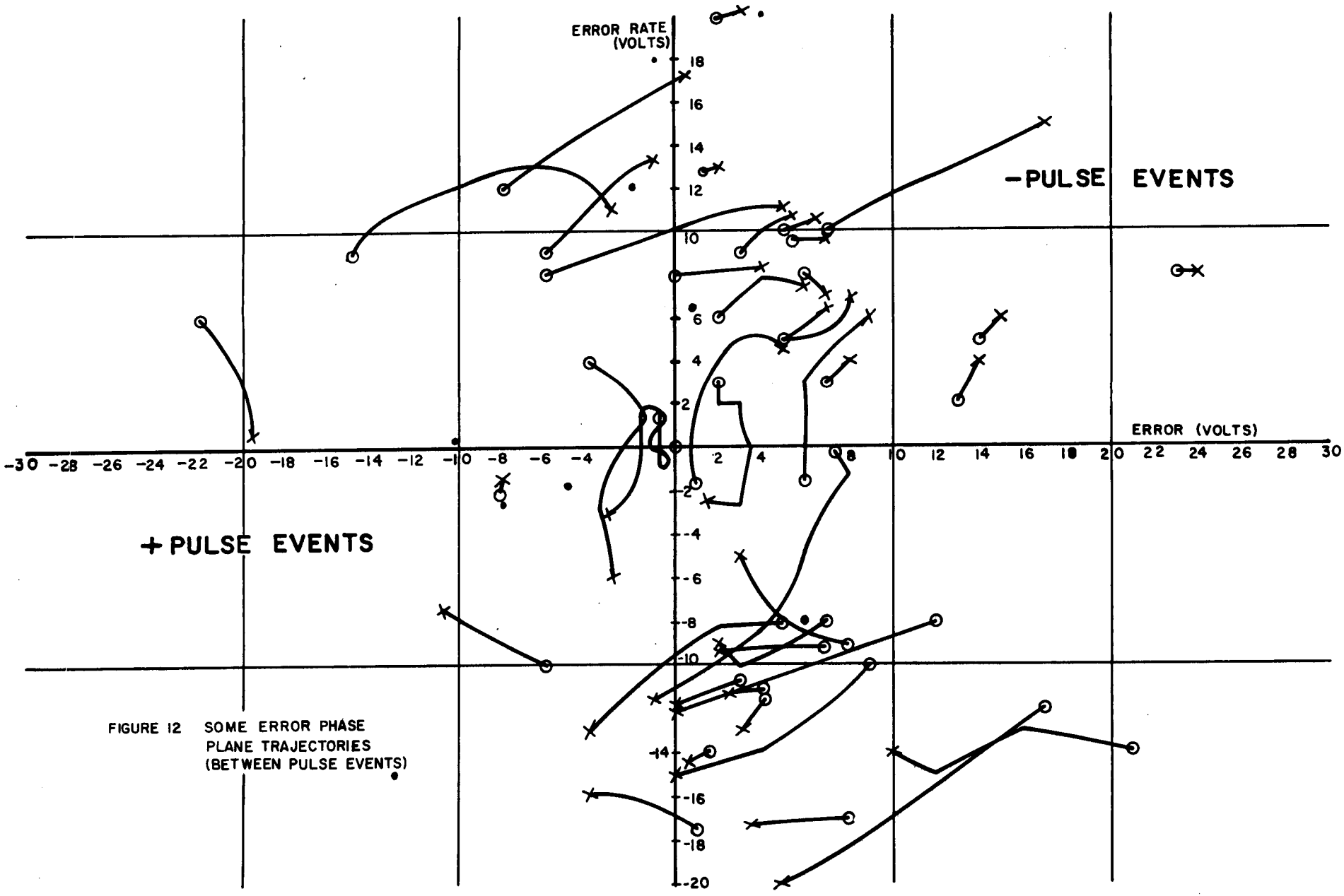


FIGURE 12 SOME ERROR PHASE PLANE TRAJECTORIES (BETWEEN PULSE EVENTS)

FIGURE 13 - DISTRIBUTION FUNCTION OF PULSE INTERVALS

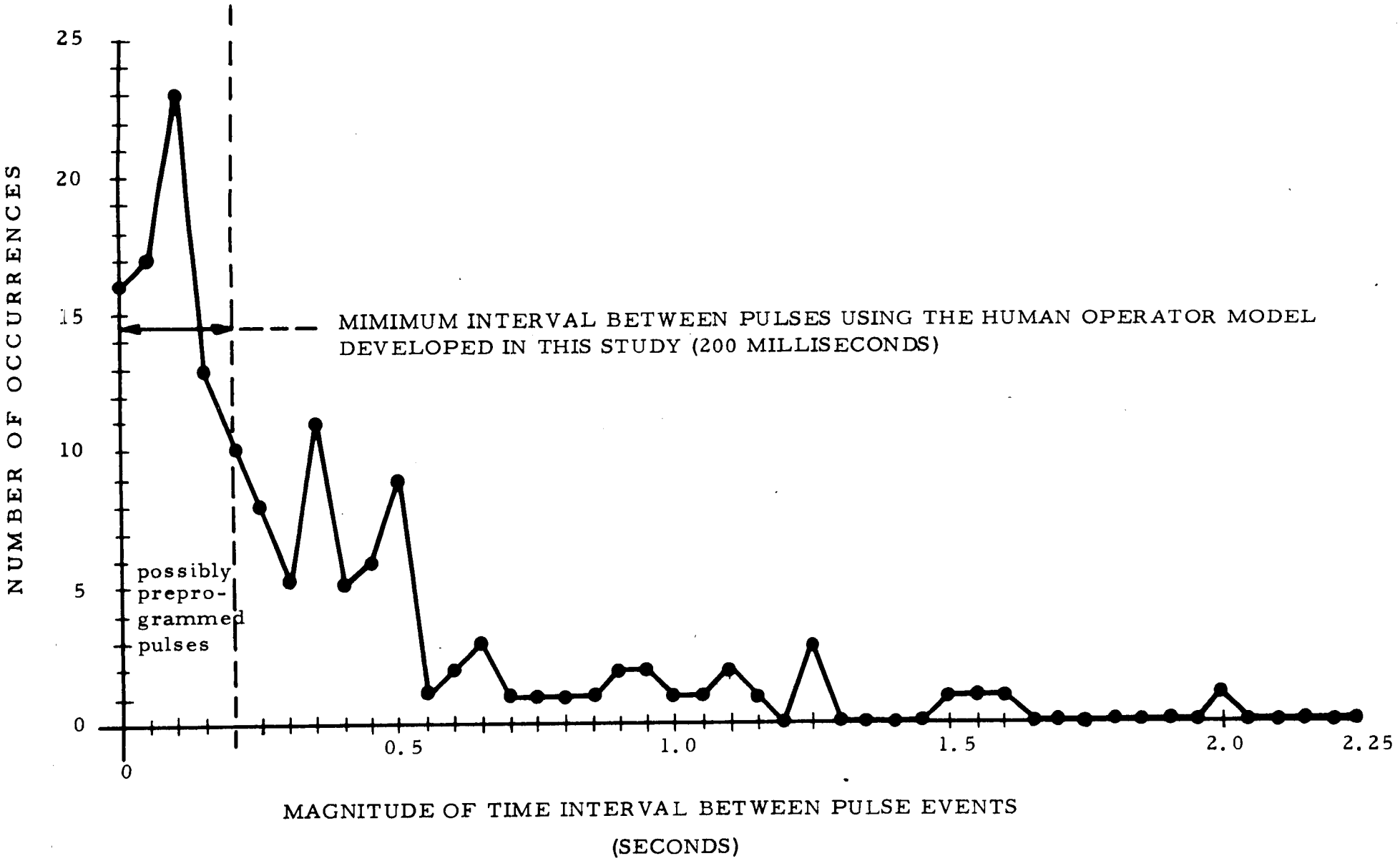

FIGURE 14 - PULSE INTERVAL CRITERION FUNCTION
OVER THE R, θ PARAMETER SPACE

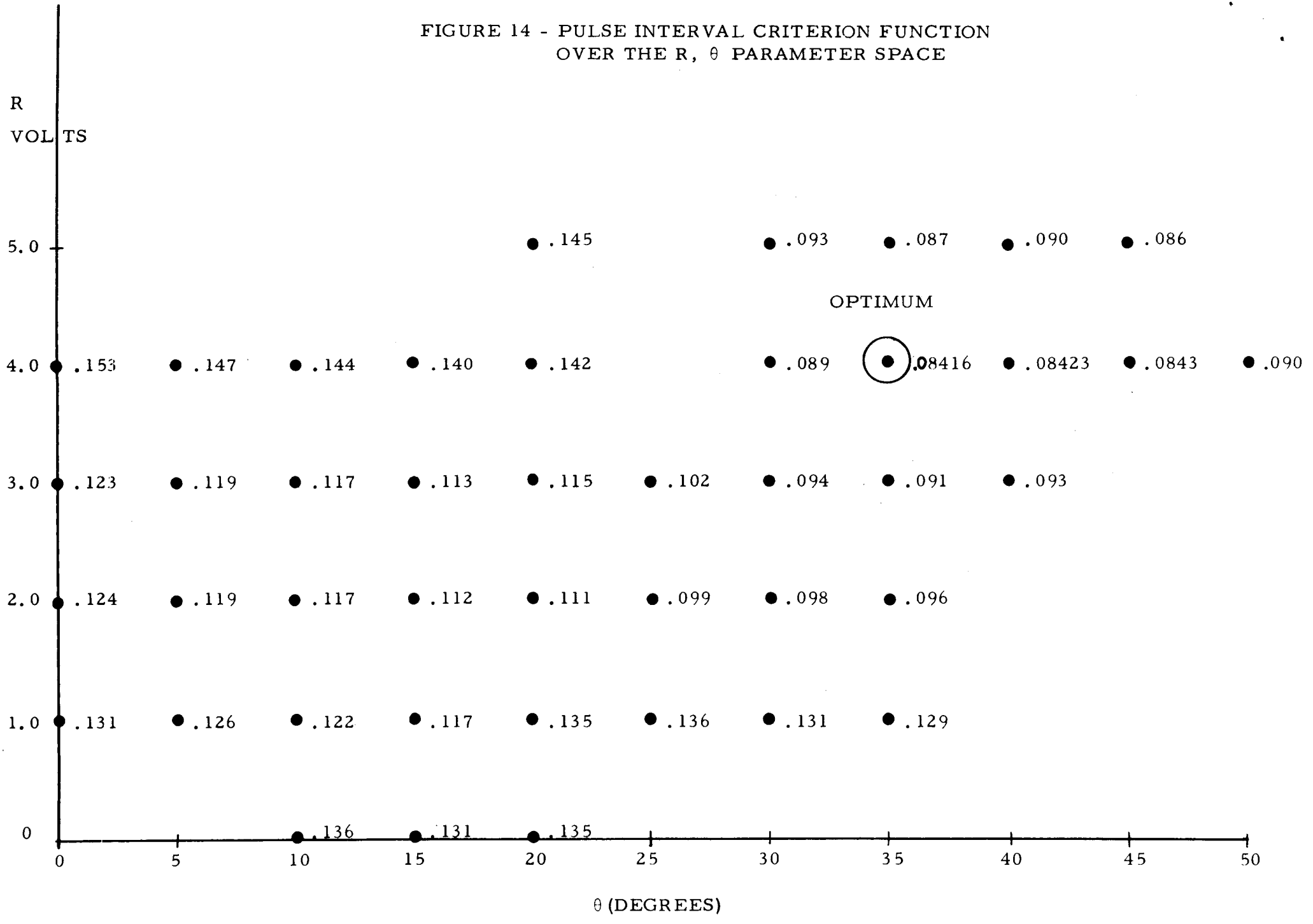

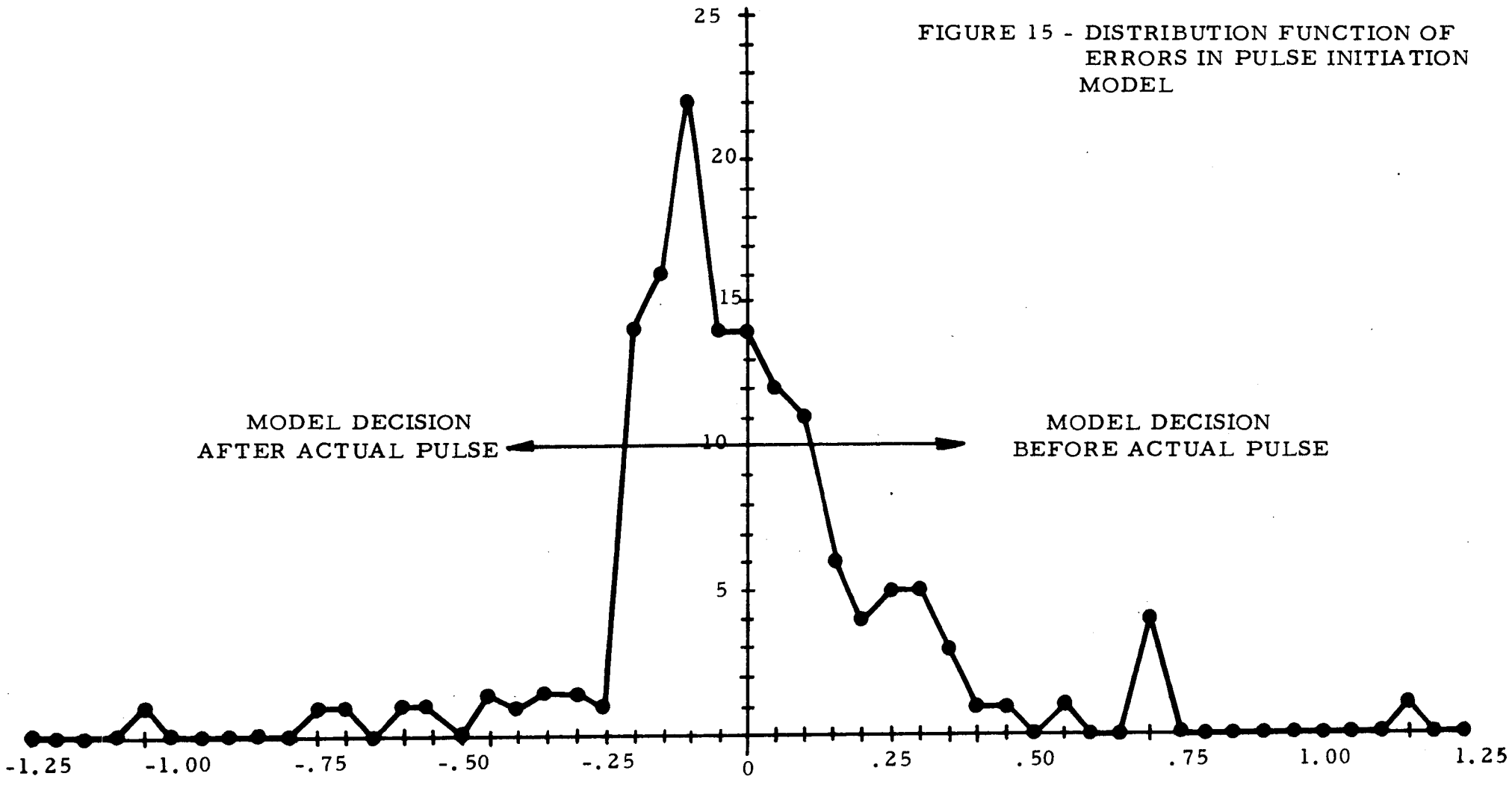


FIGURE 15 - DISTRIBUTION FUNCTION OF ERRORS IN PULSE INITIATION MODEL

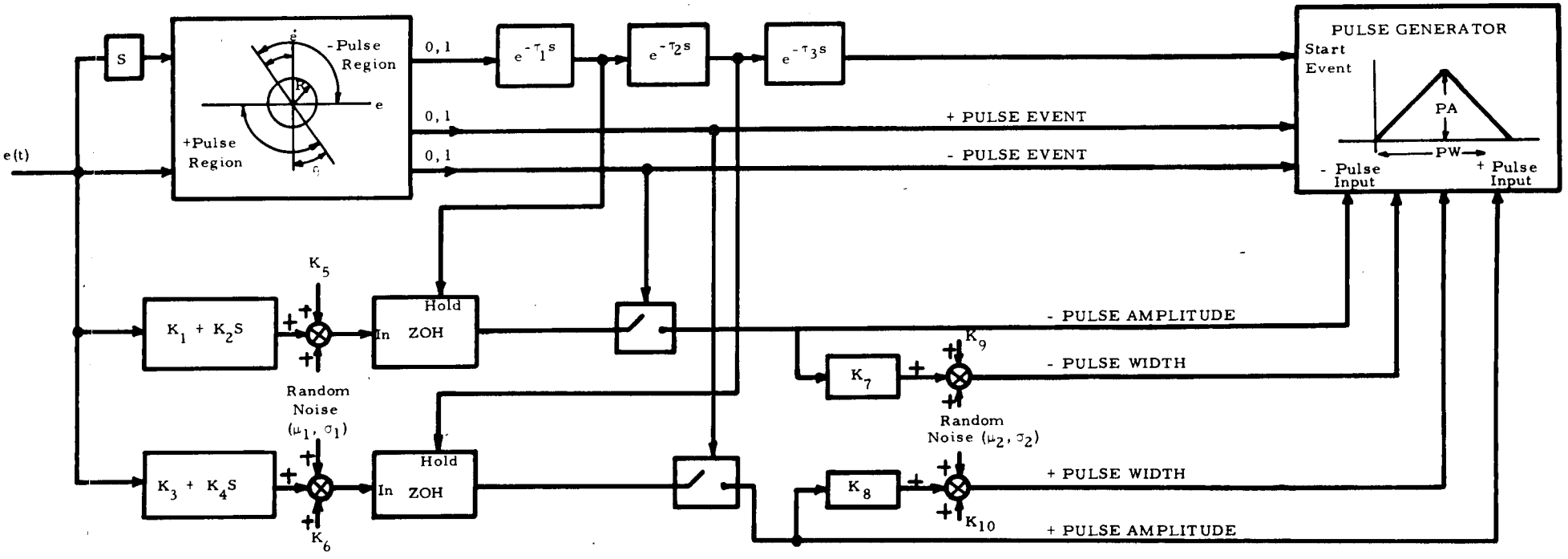


FIGURE 16A STRUC TURE OF HUMAN OPERATOR MODEL

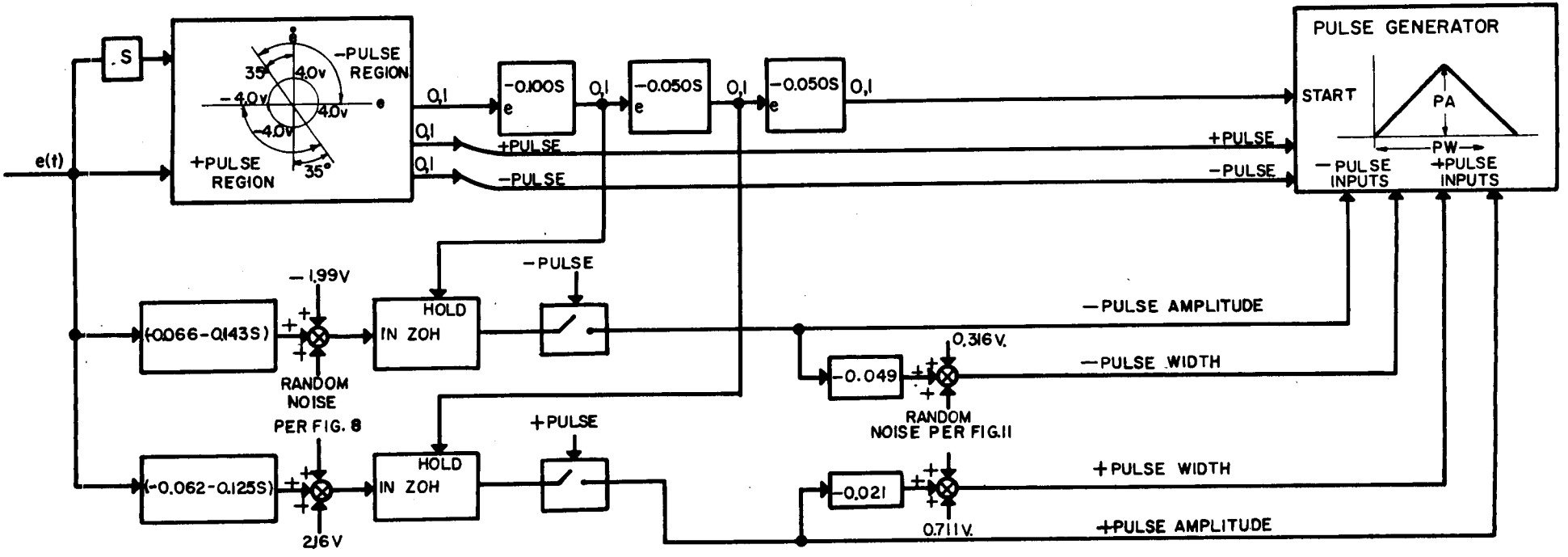


FIGURE 16 B COMPLETE HUMAN OPERATOR MODEL


USG
Engineering